Using the wavelet transform to process data from experimental studies of the discontinuous plastic deformation effect

Peter V. Trusov
Department for mathematical modeling of systems and processes, Perm National Research Polytechnic University, Perm, Russia
tpv@matmod.pstu.ac.ru, https://orcid.org/0000-0001-8997-5493

Evgeniia A. Chechulina
Ural Research Institute of Composite Materials, Perm, Russia
zhenya-chechulina@yandex.ru, https://orcid.org/0000-0003-4834-7911

Roman M. Gerasimov
Department for mathematical modeling of systems and processes, Perm National Research Polytechnic University, Perm, Russia
RMGerasimov@pstu.ru, https://orcid.org/0000-0001-6008-2288

Valeriy E. Vildeman, Mikhail P. Tretyakov
Center of Experimental Mechanics, Perm National Research Polytechnic University, Russia
wildemann@pstu.ru, http://orcid.org/0000-0002-6240-4022
cem_tretyakov@mail.ru, http://orcid.org/0000-0001-6146-6769

KEYWORDS. Discontinuous plastic deformation, Portevin – Le Chatelier effect, experimental research results, Digital Image Correlation method, wavelet analysis.

Citation: Trusov P.V., Chechulina E.A., Gerasimov R.M., Vildeman V.E., Tretyakov M.P., Using the wavelet transform to process data from experimental studies of the discontinuous plastic deformation effect, Frattura ed Integrità Strutturale, 68 (2024) 159-174.

Received: 21.11.2023
Accepted: 13.01.2024
Published: 27.01.2024
Issue: 04.2024

INTRODUCTION

A large number of studies have been devoted to the experimental study of spatiotemporal inhomogeneity during plastic deformation of macrospecimens made of various alloys, which arises under monotonic loading. Effects such as discontinuous yielding (the Portevin – Le Chatelier (PLC) effect) are of interest both from a fundamental point of view and from the point of view of creating correct mathematical models to describe the materials behavior. The PLC effect has a negative impact on the characteristics of finished products in the aircraft and motor industries: it reduces fatigue strength, corrosion resistance, and aerodynamic characteristics.

The manifestation of the effect of discontinuous yielding under loading turns out to be sensitive to variations in such impact parameters as strain rate, experimental temperature, and accumulated plastic strain. Discontinuous yielding as a phenomenon of complex spatiotemporal dynamics, arising as a result of the collective moving of main deformation carriers (dislocations) and their interaction with defects of various natures, manifests itself at various scale levels. For experimental study and description of observed multi-scale processes, it is necessary to use methods that, in terms of resolution, correspond to the considered scale of the supposed physical carriers of discontinuous yielding and the inhomogeneities manifested during their activation.

Brief literature review

Various measurement methods are used to analyze the Portevin – Le Chatelier effect. Of great importance are optical methods and non-destructive testing tools that allow non-contact recording of spatial heterogeneity of plastic yielding at the mesolevel, for example, the method of digital image correlation (DIC) [1-7]; digital speckle interferometry [2, 8, 9, 10], which allows to record localized deformation areas "in situ"; digital infrared thermography [8, 11, 12].

Among research methods on a microscale, one of the most common is electron microscopy [13-17], which allows to observe and analyze the structure of materials at the micro level. There are various microscopy techniques including optical microscopy, electron microscopy, atomic force microscopy.

In work [18], a separate section is devoted to the consideration of experimental methods for studying the PLC effect, classified into the following groups of methods: optical, thermographic, acoustic emission, measuring changes in magnetic and electric fields, electrochemical. To analyze the PLC effect, X-ray diffraction [19] and spectral analysis [20], acoustic emission [21-24], and laser strain measurement [3] are widely used.

In real technological processes, the material at macro level experiences complex loading; despite this, to study the PLC effect, the vast majority of experiments are carried out under uniaxial loading (most often – tension or compression loading, less often - simple shear loading), however, in recent years, works by domestic and foreign researchers have appeared, which consider more complex loading paths [25, 26, 27]. Experimental studies on nonproportional elastoplastic deformation of materials under complex stress-strain states is an important part of creating new and verifying existing mathematical models of plasticity theory.

A number of authors [18] explain the formation of deformation bands by the collective motion of dislocations interacting with long-range stress fields. Plastic deformation is concentrated mainly in shear bands, the occurrence of which precedes the stress drops. After passing the shear band along the length of the specimen, a phase of rapid increase in stress and lattice distortion begins (up to the moment of a new band nucleation). Based on the available experimental data on uniaxial loading, three main types of the PLC effect manifestation are distinguished [28-34]: 1) type A - characterized by repeated stress "jumps" (hereinafter jumps) of small amplitude and average frequency of stress intensity in relation to the smoothed curve [12, 15, 35, 36]; 2) type B – deformation bands appear and disappear in an oscillating or intermittent mode with a high frequency, propagating along the specimen (stop-and-go) with a greater amplitude than type A jumps [11, 37-39]; 3) type C – bands appear (and disappear) randomly along the length of the specimen with low frequency and high amplitude [15, 40-42]. In field experiments, various combinations of these three types are observed [43]. Type A is realized at relatively high strain rates and low temperatures, type C is characteristic of relatively low strain rates and high temperatures, and for intermediate ranges of strain rates and temperatures, type B of the PLS effect occurs. Fig. 1 shows a schematic representation of the «uniaxial stress σ – uniaxial strain ε» diagrams in the range of the PLC effect manifestation.

This paper presents the results of the experimental study of the Portevin–Le Chatelier effect, obtained in experiments with thin-walled tubular specimens made of aluminum alloy AMg6M at room temperature. Deformation diagrams were obtained during uniaxial tension, shear, proportional and nonproportional loading of specimens, the inhomogeneity of strain fields and their rates was shown, illustrating the manifestation of the Portevin – Le Chatelier effect under conditions of complex loading of thin-walled tubular specimens.

The using of wavelet analysis for processing experimental data allows to qualitatively and quantitatively present the obtained results in a compact form and to analyze them.

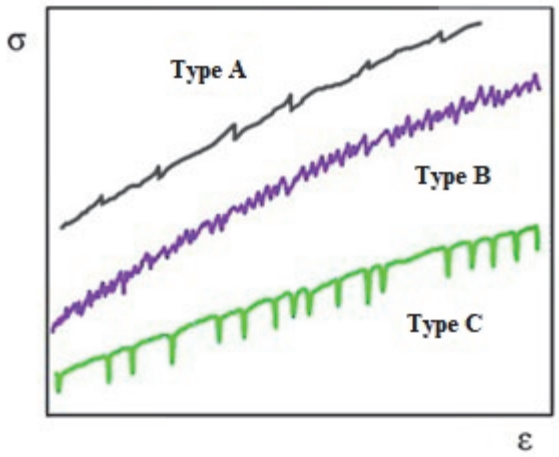

Figure 1: Schematic representation of the stress-strain diagram, depending on the type of the PLC effect manifestation.

METHODOLOGY FOR CONDUCTING FULL-SCALE EXPERIMENTS

Sample material and geometry

Structural aluminum-magnesium alloy in as-supplied state (tube workpiece with outer diameter Ø28 mm, wall thickness 5 mm) was selected as the test material. Tab. 1 presents the alloy chemical composition by weight, according to National State Standard GOST 4784-97.

Al	Mg	Mn	Fe	Si	Zn	Ti	Cu	Be
92.55	6.12	0.84	0.27	0.17	0.005	0.039	0.001	0.005

Table 1: Chemical composition of the alloy used (in %).

The choice of AMg6M alloy was determined by the importance of the problem of studying its deformation behavior stability in connection with its widespread use in aircraft engineering, shipbuilding, the chemical industry and transport engineering. Cutting out of thin-walled tubular test specimens was carried out on CNC-controlled chuck-and-center lathe with numerical control as per GOST Standart 25.505-85 according to the sketch shown in Fig. 2. The surface roughness after specimens fabrication was Ra 2.5. To achieve the microstructure homogeneity and relieve residual stresses, AMg6M alloy specimens were annealed in a PM-14 muffle furnace at 400°C for 3 hours and cooled in the furnace to room temperature.

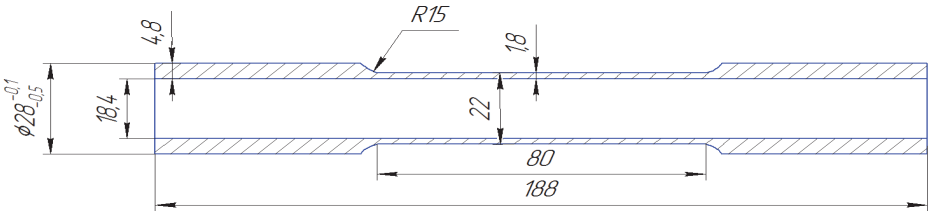

Figure 2: Sketch of a thin-walled tubular test specimen.

Equipment and means of registration

Mechanical testing was implemented on the Instron 8850 two-axis servo-hydraulic testing system. The maximum loads were 100 kN under tension/compression and 1000 Nm under torsion. The range of allowed displacement u was ± 75 mm along the tension/compression axis, and for torsion angles φ it was ± 45°. Hydraulic collet-type grippers were used to fixate the specimens in the testing machine. The test was controlled according to kinematic parameters using a two-axis mounted extensometer.

The displacement and deformation fields were recorded using the Vic 3D Correlated Solutions video system; the mathematical apparatus for processing the recorded signals is based on the method of Digital Image Correlation, with a set of high-resolution cameras (16 MP). The shooting speed was 3 frames per second.
Mechanical tests of thin-walled cylindrical specimens of aluminum-magnesium alloy AMg6M were carried out according to the loading program given in Tab. 2.

No.	Test type	Test parameters	Discontinuous yielding type observed (A, B, C; see Fig. 1)	Specimen No.
		Simple loading		
1	Uniaxial tension	$\dot{\varepsilon} = 5.4 \cdot 10^{-4}\ 1/s$ $\dot{\varepsilon}_e = 5.4 \cdot 10^{-4}\ 1/s$	Type B	1 2
2	Torsion	$\dot{\gamma} = 9.35^{-4}\ 1/s$ $\dot{\varepsilon}_e = 5.4 \cdot 10^{-4}\ 1/s$	Ill-defined discontinuous yielding Type A	3 4
3	Proportional loading	$\dot{\varepsilon} = 5.85 \cdot 10^{-4}\ 1/s$ $\dot{\gamma} = 0.675 \cdot 10^{-4}\ 1/s$ $\dot{\varepsilon}_e = 5.4 \cdot 10^{-4}\ 1/s$	Type B	5 6
		Combined loading (Changing of path when $\varepsilon > \varepsilon_{cr}$)		
4	Uniaxial tension → torsion	$\dot{\varepsilon} = 5.389 \cdot 10^{-4}\ 1/s$ before elongation 5.05 mm → $\dot{\gamma} = 9.35^{-4}\ 1/s$	Didn't manifest itself → Type A+C	7
5	Torsion → Uniaxial tension	$\dot{\gamma} = 9.35^{-4}\ 1/s$ → $\dot{\varepsilon} = 5.389 \cdot 10^{-4}\ 1/s$	Type A → Type B	8
6	Proportional loading → tension	$\dot{\varepsilon} = 5.389 \cdot 10^{-4}\ 1/s +$ $\dot{\gamma} = 0.675 \cdot 10^{-4}\ 1/s$ → $\dot{\varepsilon} = 5.389 \cdot 10^{-4}\ 1/s$	Type B → Type C with the transition to a mixed type (B+C)	9

Table 2: Mechanical testing program.

The tests were carried out at room temperature 21.2°C. Figs. 3-12 show the resulting diagrams (curves). Part of the data on specimens loading (during tensile and torsion tests) was presented in [44].

EXPERIMENTAL RESULTS

Simple loading

Strain-stress diagrams for thin-walled cylindrical specimens under uniaxial tension, plotted using data obtained from the video system "virtual extensometer", are shown in Fig. 3.

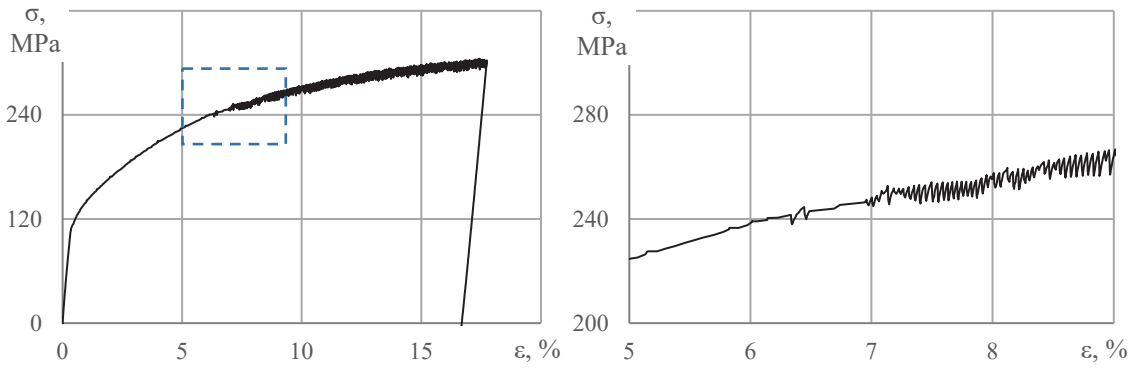

Figure 3: Stress-strain diagram (deformation curve) (*left*) and an enlarged fragment of the curve (*right*) of specimen No. 1 under uniaxial tension.

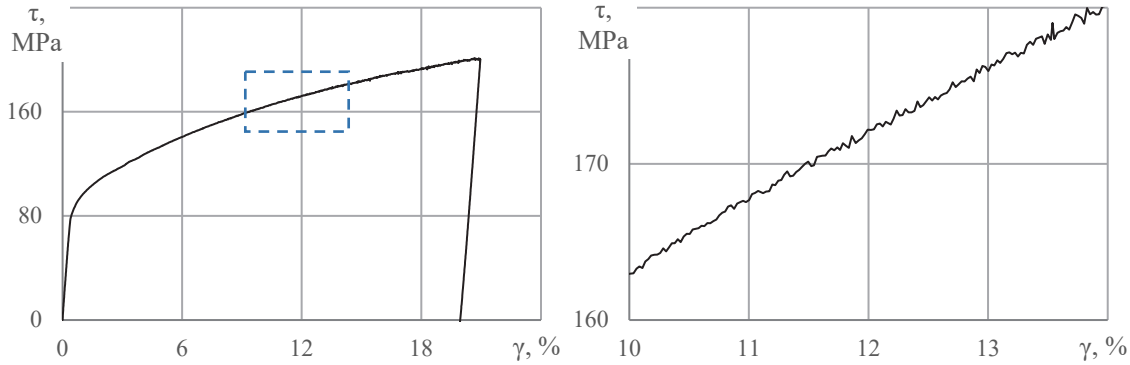

Figure 4: Torsional deformation curve (*left*) and an enlarged fragment of the curve (*right*) (No. 3).

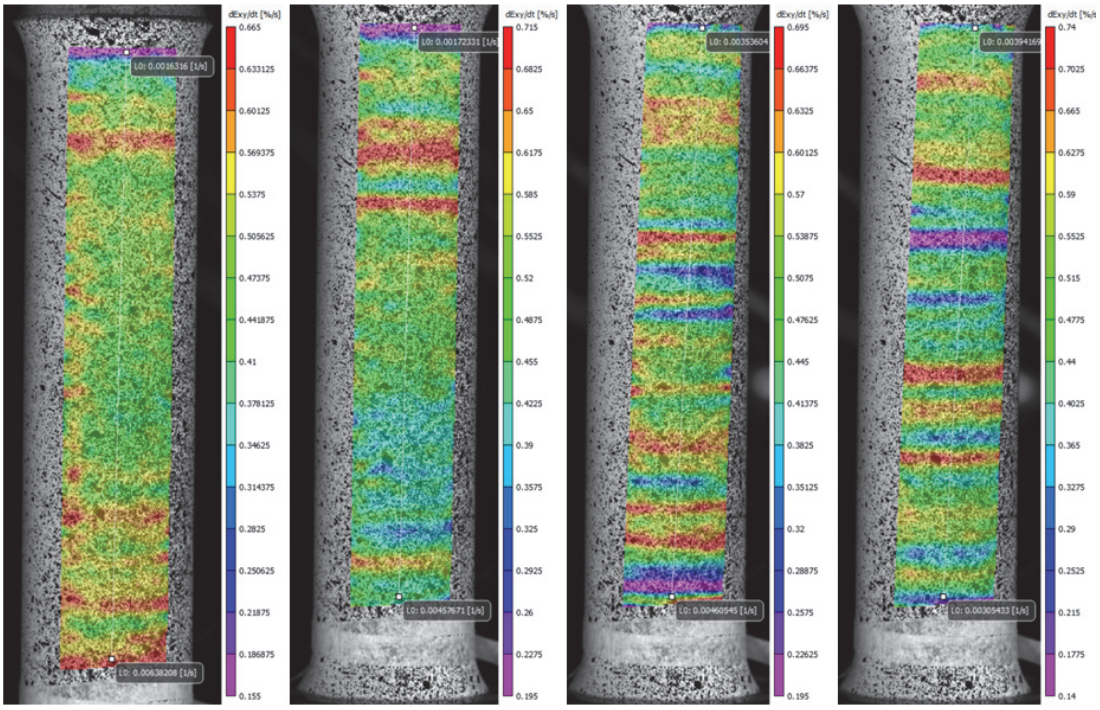

a *b* *c* *d*

Figure 5: Inhomogeneous fields of local strain rates (*a* – 13 sec, *b* – 14 sec, *c* – 16.5 sec, *d* – 17 sec), corresponding to the intensity values of the accumulated strain (*a* – 8.03%, *b* – 8.2%, *c* – 10.2%, *d*– 10.3%) for specimen No. 4 under torsion.

A similar graph was obtained for specimen No. 2 (specimen numbering is given in Tab. 2), while the values of the critical strain, which correspond to the onset of discontinuous yielding and initiation of deformation bands of the PLC effect of specimens No. 1 and No. 2 during a uniaxial tensile test, are equal to 5.59 % and 5.91%, respectively. Until this value is reached, areas of localized plastic yielding of the material are not detected on the surface of the specimens. The relative difference of these values, related to the maximum value of the critical deformation (in specimen No. 2), was about 5.4%. On the stress-strain diagram of specimen No. 1, one can note a single stress drop (at strain value of 5.59%), characterizing the beginning of the PLC effect manifestation.

In torsion tests (specimen No. 3) determining the value of critical deformation (ε_{cr}) is difficult due to the small amplitude of jumps on the diagram (Fig. 4, 5). Based on the video system data, there was definitely a critical value of shear strain γ_{cr} equal to 1.69%, corresponding to a stress intensity of 104 MPa.

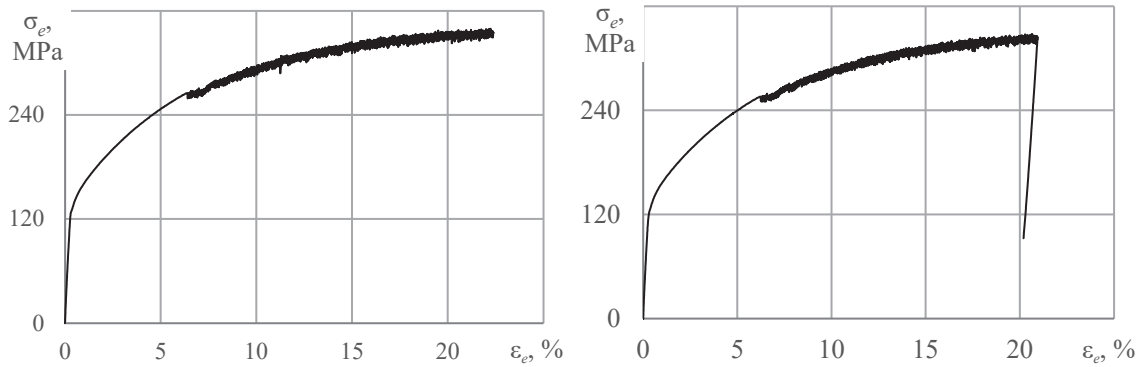

Figure 6: Deformation curve "stress intensity σ_e – accumulated strain intensity ε_e" during combined tension with torsion of specimens No. 5 (a) and No. 6 (б), respectively.

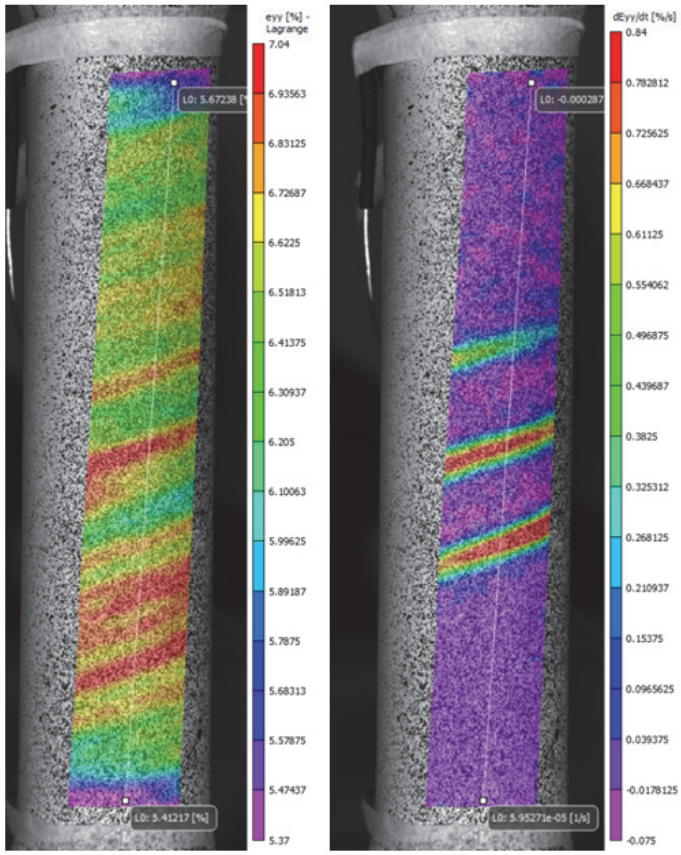

a *b*

Figure 7: Inhomogeneous fields of local rates of longitudinal strain and longitudinal deformations (*a* – 121 sec, *b* – 250 sec), corresponding to the intensity values of the accumulated strain (*a* – 9.62%, *b* – 19.88%) for specimen No. 5 under proportional load.

For specimen No. 4, a similar graph was obtained for a pure shear test with remounting the specimen, when maximum torsion angle of the test system was reached, and with repeated loading. As an example, inhomogeneous fields of local rates of longitudinal deformation are given (Fig. 5), illustrating the manifestation of the Portevin – Le Chatelier effect under conditions of torsion of a thin-walled tubular specimen made of AMg6M alloy.

Proportional loading (tension with torsion) was implemented on specimens No. 5 and No. 6, the deformation diagrams are presented in Fig. 6. Inhomogeneous fields of local rates of longitudinal strain and longitudinal strains for specimen No. 5 are presented in Fig. 7.

Analysis of the shear band patterns revealed significant differences in the distribution of shear bands all over the specimen under torsion (see Fig. 5) compared to uniaxial tension [44] and proportional loading (see Fig. 7). Plastic deformation at the initial stage (nucleation of deformation bands) occurs along the action planes of maximum tangential stresses. The pattern of propagation of deformation bands in the specimen under proportional and uniaxial loading has a similar character. It should be noted, that the angle between the Portevin-Le Chatelier band and the uniaxial tension axis in case of proportional loading takes the value ±56°. The shear bands during torsion are oriented perpendicular to the axis of the specimen; accordingly, the shear bands propagate along the axis of the specimen.

Complex loading

For specimens No. 7, 8, 9, complex loading tests were carried out: a) uniaxial tension with a further torsion; b) torsion followed by tension; c) proportional loading (tension + torsion) followed by tension, respectively. The change in strain paths (deformation trajectories) occurred with accumulated strains exceeding ε_{cr}. Fig. 8 shows strain paths under complex loading in the coordinates "axial strain - shear strain" for all specimens.

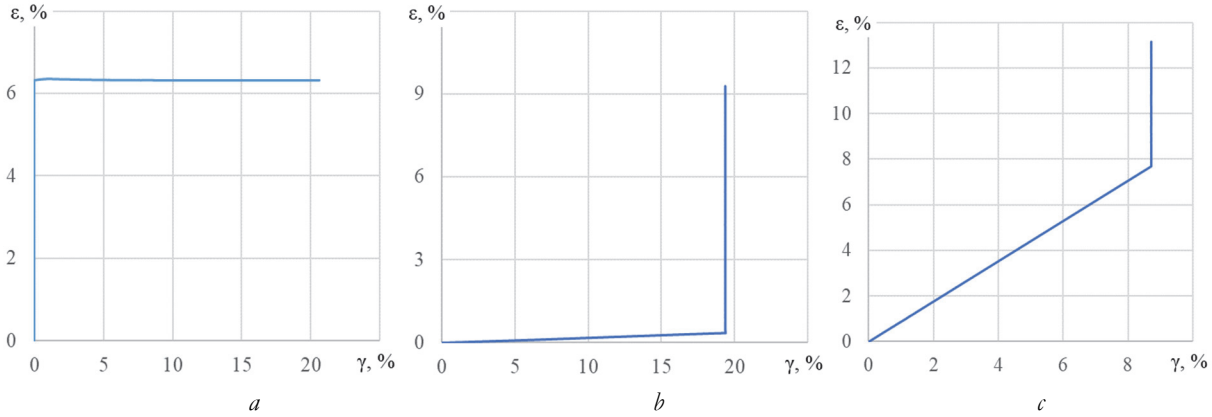

Figure 8: Strain paths for specimens No. 7 (*a*), 8 (*b*), 9 (*c*).

Deformation curve of specimen No. 7 in the coordinates "stress intensity – accumulated strain intensity" is presented in Fig. 9.

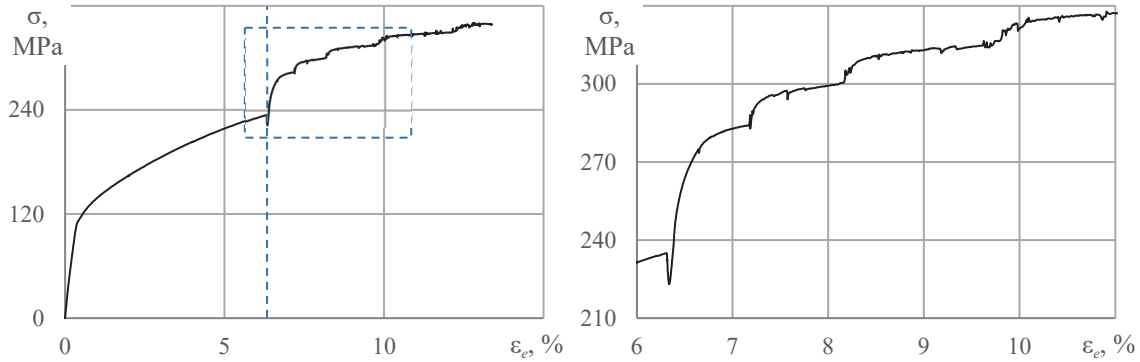

Figure 9: Diagram "stress intensity – accumulated strain intensity" (*left*) and an enlarged fragment of the curve (*right*) for complex loading of specimen No. 7 under uniaxial tension followed by torsion. Dashed line indicates the moment of the loading path changing.

The critical strain for the onset of manifestation of the Portevin – Le Chatelier effect in uniaxial tensile tests for specimens No. 1 (Fig. 3) and No. 2 was 5.59% and 5.91%, respectively. The loading path changing of specimen No. 7 realized at strain

level greater than critical strain value ($\varepsilon' = \varepsilon_{cr}$ (tension) +1%= 6.31%). However, the PLC effect did not appear until the deformation mode changed, which indirectly indicates the dependence of critical strain on strain history.
Fig. 10 shows a set of longitudinal deformation profiles for specimen No. 7; the deformation profile, which was plotted at the moment of the loading path changing from uniaxial tension to torsion, is highlighted in red.

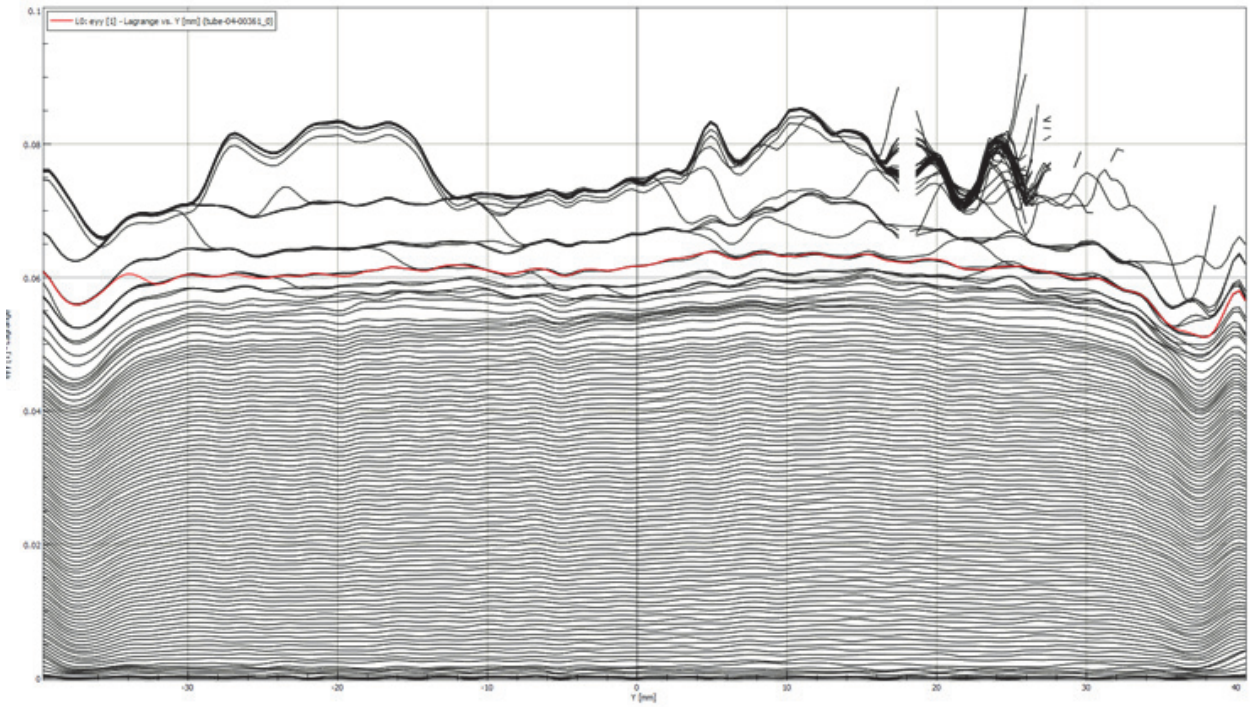

Figure 10: A set of longitudinal strain profiles for specimen No. 7 under uniaxial tension followed by torsion.

Thus, the change of loading mode was completed before the initiation of the discontinuous yield effect, which is confirmed by the absence of load drops (waves) on the loading diagram (Fig. 9). Based on these profiles (Fig. 10), we can conclude that path changing did not lead to the simultaneous emergence of spatiotemporal inhomogeneity during loading. The deformation diagram of specimen No. 7 (Fig. 9) clearly shows single stress drops (kinks), characteristic of type C of the PLC effect manifestation, up to strain value of 9.46%; with further twisting of the traverse and increasing the applied torque in the specimen, single load (stress) jumps characteristic of type A of the PLC effect are recorded on the curve, alternating with stress drops of type C of the PLC effect. Consequently, under complex loading, implemented according to the program of uniaxial tension with subsequent torsion, a mixed type of discontinuous yield appears (A+C).
The area of sharp strengthening (Fig. 9) with a change in the deformation mode is probably associated with the intensive formation of Lomer – Cottrell barriers.
Test results for loading with "torsion → tension" path for specimen No. 8 are presented in Fig. 11. The moment of loading path changing is highlighted by the dashed line. The loading mode changed at strain level exceeding the critical strain values for the onset of the Portevin – Le Chatelier effect manifestation for torsion. The deformation profile shows bands of A-type of the PLC effect, which arose before the moment of the kink on the strain path (Fig. 11). It should be noted that after the transition from torsion to uniaxial tension, the effect of discontinuous yielding is not observed for some time. With further stretching of the specimen, processes of localization of plastic yielding are again recorded on the surface of the material under conditions of manifestation of the PLC effect, characteristic of type B.
Test results for loading with "proportional loading → tension" path (Fig. 8*c*) for specimen No. 9 are presented in Fig.12. The loading path changed after reaching the critical strain of the discontinuous yield effect manifestation for proportional tension. The moment of changing the loading path is indicated by the dashed line.
The deformation diagram of specimen No. 9 under proportional loading followed by tension (Fig. 12) before changing the loading path has stress drops of small amplitude. The kinetics of band formation in this case corresponds to discontinuous yielding of type B. After the transition from proportional biaxial loading to uniaxial tension, discontinuous yielding characteristic of mixed type (B+C) is observed on the diagram. In this case, discontinuous deformation under conditions

of uniaxial tension after proportional loading differs in the frequency and amplitude of jumps from the diagram obtained under simple loading (under uniaxial tension in Fig. 3).

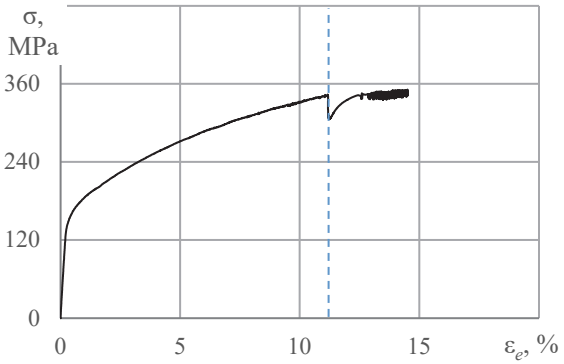

Figure 11: Diagram "stress intensity – accumulated strain intensity" for specimen No. 8 under torsion with subsequent tension.

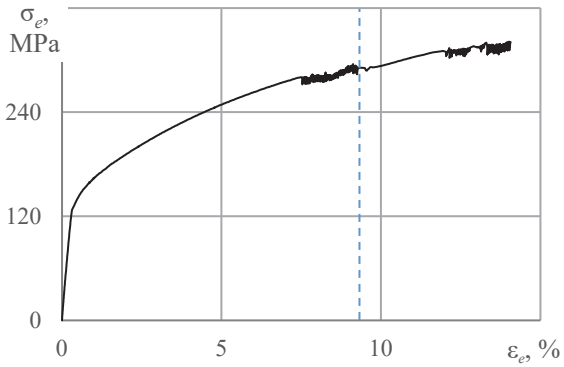

Figure 12: Deformation diagram "stress intensity – accumulated strain intensity" for specimen No. 9 under proportional biaxial loading with subsequent tension.

On all deformation curves, the moments of the beginning of unstable deformation or of the first stress drop occurrence were found. Under uniaxial loading (Fig. 3), a single jump is observed, characterizing the occurrence of plastic yielding instability associated with the occurrence of collective separation of dislocations from clouds of impurity atoms, followed by a transition to the discontinuous deformation mode of type B. Proportional loading is also characterized by type B of the PLC effect, while the jumps amplitude on the diagram is approximately two times higher than jumps amplitude under uniaxial loading (Fig. 6). Determining the type of the PLC effect during torsion (Fig. 4) is complicated by small amplitude of jumps on the deformation diagram; based on the nature of the diagram, this case can be classified as type A.

WAVELET TRANSFORM FOR EXPERIMENTAL DATA ANALYSIS

A wavelet is a function ψ defined on the entire numerical axis, having zero average and a fairly rapid decrease at infinity. Transforms performed using wavelets are called wavelet transforms (WT) [45, 46]. WT is widely used for signal analysis, in particular, for filtering, information compression, etc. [47, 48]. Compared to the Fourier transform (FT), which decomposes the signal into a basis of sines and cosines, i.e. functions localized in Fourier space, WT is basis decomposition, which is formed from a function with certain properties, called the mother wavelet, using its scale changes and transfers. Each wavelet basis function is characterized by a certain scale (frequency) and localization in time. WT allows to obtain a sweep of the original signal simultaneously in both time and frequency, which cannot be obtained using FT.

To perform the WT, the researcher needs to determine the base (mother) wavelet - function (1), which is the prototype for the entire family of wavelets (2):

$$\psi = \psi(t) \tag{1}$$

$$\psi_{ab}(t)=\frac{1}{\sqrt{a}}\psi\left(\frac{t-b}{a}\right) \tag{2}$$

where t is time (or another non-decreasing parameter), a is the scale parameter, b is the time shift parameter.
To select the most suitable mother wavelet for wavelet analysis, several factors need to be considered:
• Signal shape: If the signal has a rapidly changing shape, then short wavelets such as Daubechies or Haar wavelets should be used [46].
• Special information: if it is necessary to select certain frequencies in a signal, then it is advisable to use wavelets that approximate these frequencies well.
• Wavelet resolution also plays an important role. If it is necessary to identify informative features of a signal, then a high-resolution wavelet should be selected, for example, the Mexican wavelet ("Hat") or the Morlet wavelet [47].
• Signal-to-noise ratio: if the signal has a high noise level, then a wavelet with good noise suppression ability should be selected, such as Dongo or Shenon wavelets.
• Tolerable computational complexity: the choice of mother wavelet may also depend on computational constraints. For example, the Haar wavelet requires less computational resources than Daubechies or "Mexican hat" wavelets [49].

Examples of functions from the "Mexican Hat" wavelet family with a mother wavelet $e^{-\frac{t^2}{2}}\left(1-t^2\right)$ and various coefficients a and b are shown in Fig. 13:

$$\psi_{ab}(t)=\frac{1}{\sqrt{a}}\exp\left(-\frac{(t-b)^2}{2a^2}\right)\left((t-b)^2-1\right) \tag{3}$$

$\psi_{ab}(t)$ $a=1, b=12$ (*blue curve*),
$\psi_{ab}(t)$ $a=2, b=12$ (*orange curve*),
$\psi_{ab}(t)$ $a=2, b=8$ (*green curve*),
$\psi_{ab}(t)$ $a=4, b=12$ (*red curve*)

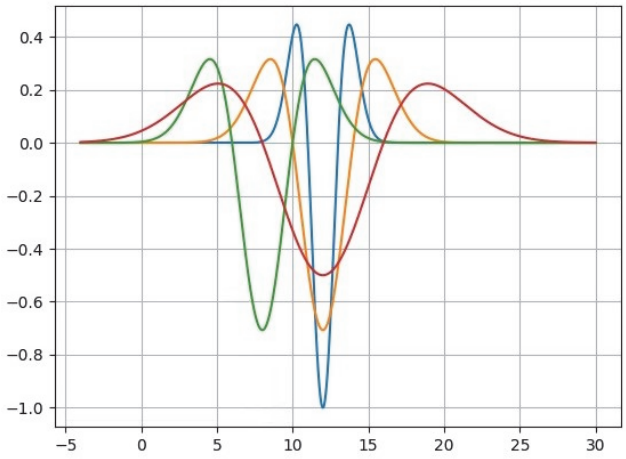

Figure13: An example of the family of wavelets "Mexican Hat", obtained from the mother wavelet.

Each wavelet of the family is specified by the shift parameter of b and scale parameter a on the time axis, thereby defining a "window" of a certain width and height in relation to the analyzed signal at a specific timepoint. Shift b controls the window moving along the signal timescale. The height of the wavelet changes by the normalizing coefficient $1/\sqrt{a}$.
The main difference between the WT and the Fourier transform (FT) is that the FT gives only averaged presentations of the analyzed signal frequencies, while the WT, due to its properties, allows to successfully and with high accuracy analyze signals in local areas, which intrinsically, in general, are nonstationary. This opportunity, when using WT, occurs because the scale a changing allows to adjust the frequency domain width, and by means of the shift b - to study the signal properties at different points.
It is known that when the effect of discontinuous plastic deformation manifests itself, sawtooth or stepped "protrusions" appear on the curve of the stress dependence on monotonically increasing strain. This paper presents some of the capabilities

of the discrete wavelet transform used to temporally filter certain types of waves on the stress-strain diagram for aluminum alloy.

Analysis of the source signal using WT is often performed using scalograms – diagrams of the WT signal coefficients absolute values depending on the wavelet scale (frequencies) and an independent parameter of the source signal (time). On wavelet transform scalograms, the values reflect the level of contribution of a component with a certain frequency and scale to the overall signal. The frequency and scale are determined by the selected wavelet. The brighter the color of the area on the scalogram, the greater its contribution to the overall signal. If the value is zero, then the corresponding component is not included in the overall signal. Using wavelet analysis, signal processing from field experiments was carried out in order to study the mechanisms of discontinuous plastic deformation. When studying the original signal using a continuous wavelet transform, a family of complex Morlet wavelets was used, which allow for good localization of signal frequencies.

Experimental data analysis involving wavelet analysis

Scalograms of loading diagrams for thin-walled specimens No. 1 and No. 2 made of aluminum alloy AMg6M during uniaxial loading tests (Fig. 3) are presented in Fig. 14. Based on the scalogram analysis it is clear that the PLC effect begins to manifest itself with an accumulated strain of 5.59% and 5.91% for specimens No. 1 and No. 2., respectively. The oscillations appearing on the diagram have a frequency from 2 to 6.5 Hz.

The highest signal power is reflected at frequency of 4 - 4.5 Hz over the entire range of deformations over which the PLC effect is realized, which allows to conclude about the most preferable frequency of jumps. The type of the PLC effect manifestation on the diagrams corresponds to type B, in which deformation bands appear and disappear in an oscillating or intermittent mode with a high frequency.

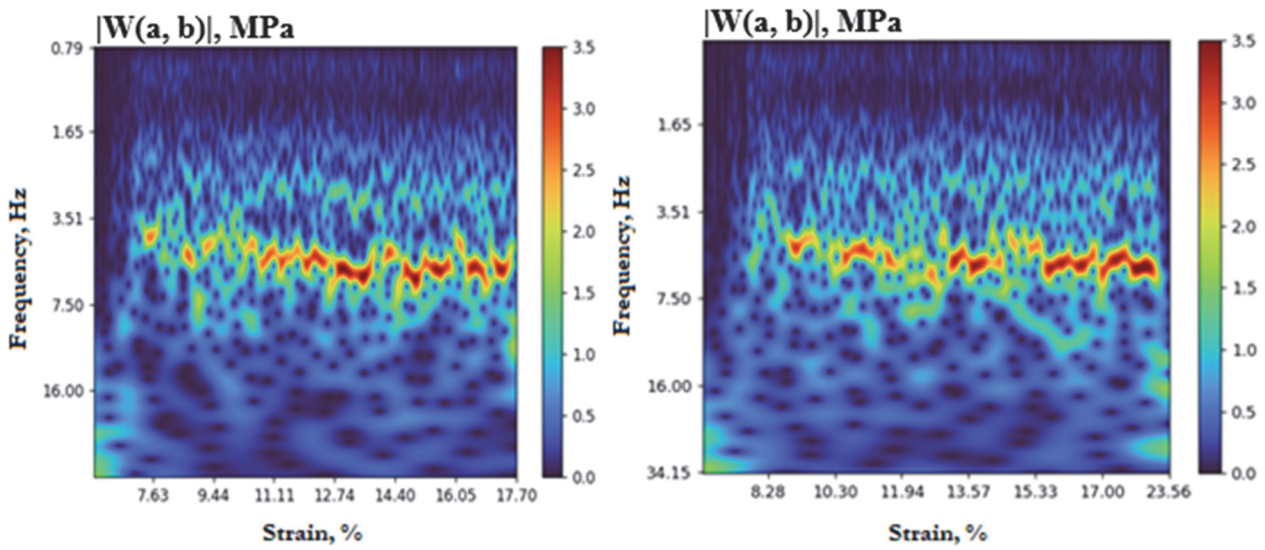

Figure 14: Loading diagram scalogram of specimen No. 1 (uniaxial tension) (*left*) and loading diagram scalogram of specimen No. 2 (uniaxial tension) (*right*).

For specimens No. 3 and No. 4, deformed by torsion (Fig. 4), a small amplitude of jumps was observed on the loading diagrams. Due to ill-defined manifestation of the PLC effect during torsion of the specimens, the scalograms did not show amplitude bursts (stress jumps on the loading diagrams are comparable to noise that is filtered out (Fig. 15)). However, using wavelet analysis, based on the analysis of the scalogram it is possible to identify a region, starting from a twist angle of 0.1 rad, where the energy of the wavelet transform increases relative to the previous region, which indicates a more obvious manifestation of the PLC effect. Note that the scale range of the scalogram for these experiments is reduced to a value of 1, since due to the smaller amplitudes of the occurring jumps, the energy of the wavelet transform in the region of the PLC effect is less than at large amplitudes (Fig. 3-5).

More intense amplitude bursts in the graph (compared to uniaxial loading, Fig. 3) are observed for the results of experiments with specimens subjected to proportional loading (specimens No. 5 and No. 6 (Fig. 6)), however, on the scalograms for

these data (Fig. 16) the signal power is less compared to that shown on the scale diagram in Fig. 14. In this case, the most pronounced frequencies of stress jumps are observed in the range of 3 – 3.75 Hz.

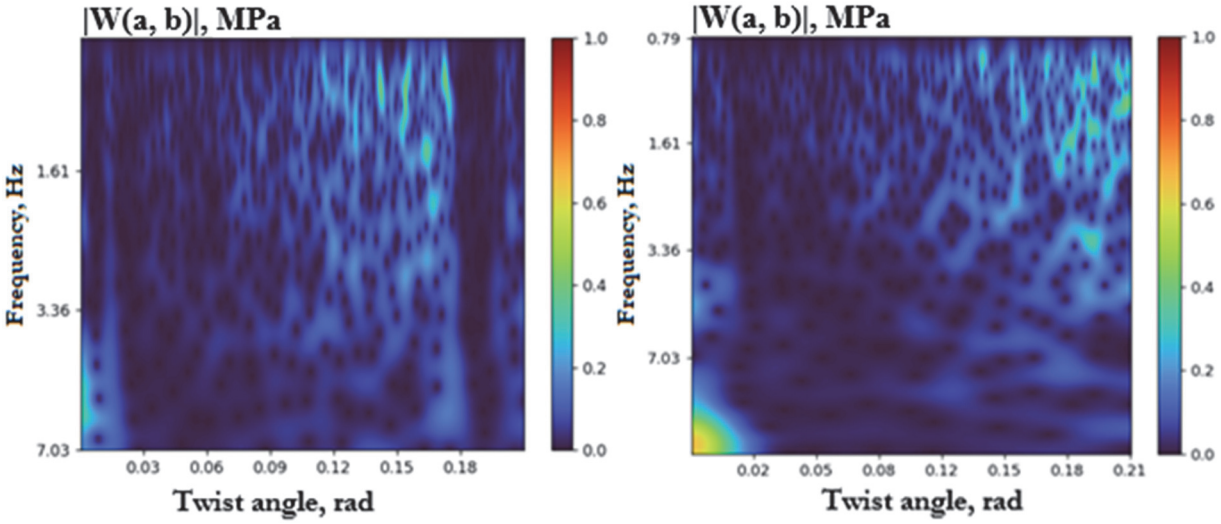

Figure 15: Loading diagram scalogram of specimen No. 3 (*left*) and No. 4 (*right*) (torsion).

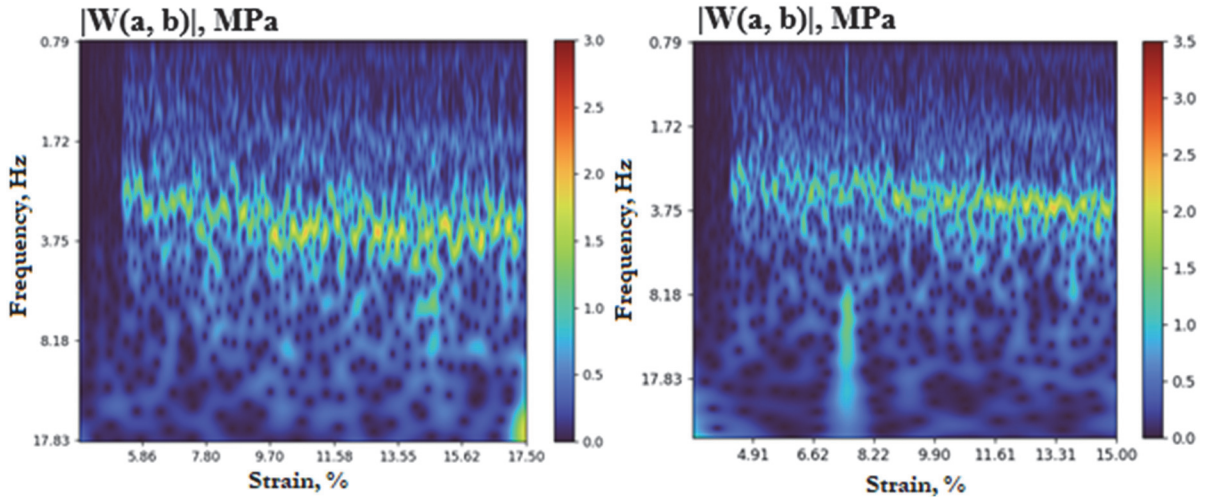

Figure 16: Loading diagram scalogram of specimen No. 5 (*left*) and No. 6 (*right*) (proportional loading).

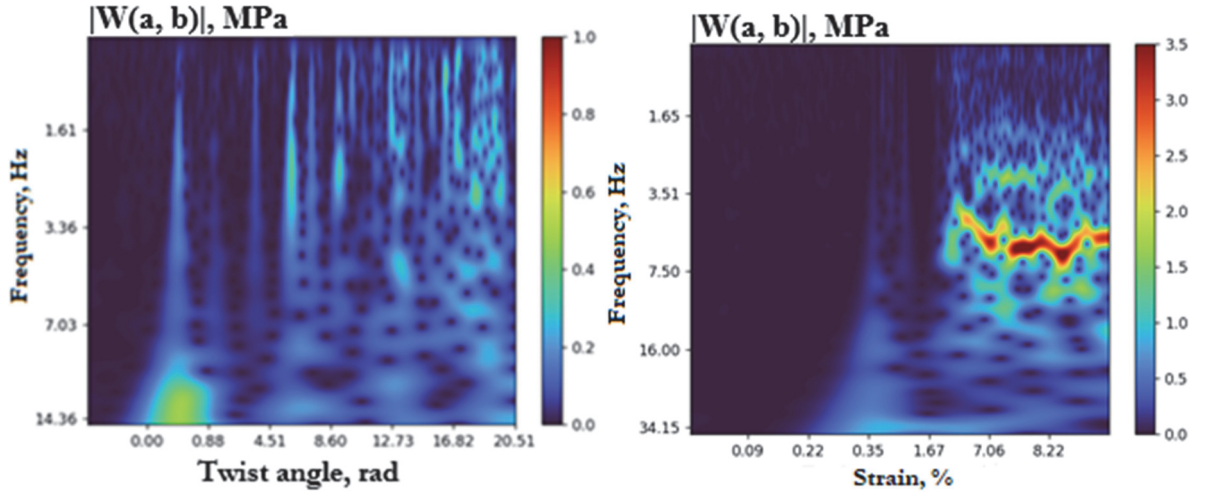

Figure 17: Loading diagram scalogram of specimen No. 7 (tension followed by torsion) (*left*) and loading diagram scalogram of specimen No. 8 (torsion followed by tension) (*right*).

For complex loading (tension followed by torsion, specimen No. 7 (Fig. 9)), the scalogram is presented in Fig. 17 (*left*). The scalogram shows that until the initial curve kinks, the PLC effect does not occur (no bursts in the initial part of the scalogram). The type of the PLC effect that appears belongs to the mixed type A + C and it is observed in the right part of the diagram, corresponding to the moment of the kink on the original curve.
For complex loading of specimen No. 8 (torsion followed by tension (Fig. 11)), scalograms were also plotted (Fig. 17 (*right*)). Type A of the PLC effect that appears, with a frequency of 3.5 Hz (in the initial section of loading, up to the deformation of 4.77%), transforms into type B with a characteristic jumps frequency of 4.3 – 8.0 Hz, which is clearly presented on the resulting scalogram.
For complex loading test (proportional tension + torsion → tension, specimen No. 9 (Fig. 12)), scalogram is presented in Fig. 18. Type B of the PLC effect that appears, with a frequency of 3.2 Hz (up to the strain of 7%), transforms into a mixed type B + C.

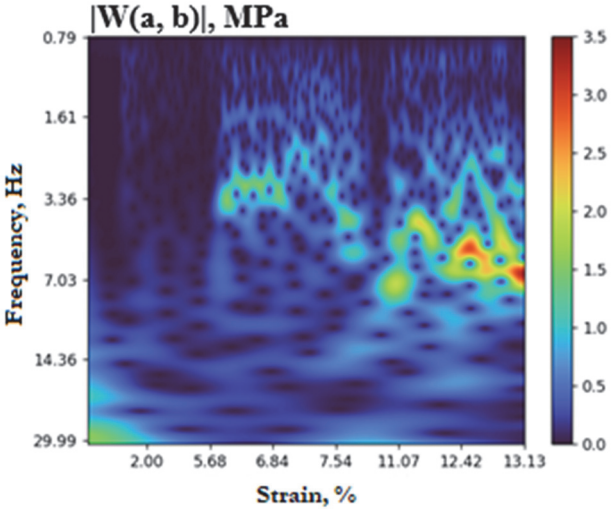

Figure 18: Loading diagram scalogram of specimen No. 9 (proportional tension + torsion followed by tension).

The using of wavelet analysis allows to identify, which frequencies in the initial signal data are most significant for this effect analyzing. High-frequency regions on the scalograms, where large values of signal power are recorded with some periodicity, are associated with the effect of discontinuous plastic deformation and indicate collective separation of dislocations from impurity atoms at times when the wavelet spectra are maximum.
Scalograms allow to carry out frequency analysis of specific dependencies and assessment of frequency changes depending on deformation. In addition, wavelet analysis of mechanical tests results makes it possible to analyze the amplitudes of individual bands depending on the deformation, since individual types of strain jumps have different frequencies. For example, type B bands are characterized by the presence of one pronounced frequency on the scalogram; type A bands, due to their lower frequency, appear as noise (low-frequency oscillations) with smaller amplitudes.

Conclusion

1. Mechanical tests of thin-walled cylindrical specimens made of aluminum-magnesium alloy AMg6M were carried out on the Instron 8850 testing system to study the PLC effect during uniaxial tension, torsion, proportional loading, as well as complex loading experiments: uniaxial tension accompanied by torsion, torsion followed by tension, proportional biaxial loading (tension - torsion) followed by tension. The fields of displacement and deformation were recorded using the Vic 3D Correlated Solutions video system, the mathematical apparatus of which is based on the method of Digital Image Correlation, with a set of high-resolution cameras (16 MP).
2. The types of the PLC effect manifestation for each type of simple loading and complex loading are determined. Proportional and uniaxial loading are also characterized by type B of the PLC effect, in this case, the amplitude of jumps in the proportional loading diagram is approximately twice as large as the amplitude of jumps under uniaxial loading. During torsion A type of the PLC effect is realized, with a small amplitude of jumps.
3. It was revealed that path changing did not lead to the simultaneous emergence of spatiotemporal inhomogeneity during loading, and the critical strain depends on the strain history.

4. Depending on the type of complex loading, various types of the PLC effect manifestation are realized. Under complex loading, implemented according to the program of uniaxial tension with subsequent torsion and "proportional loading → tension", a mixed type of discontinuous yield appears (A+C) and (B+C), respectively. Under complex loading "torsion → tension" appear type B of the PLC effect.
5. Using wavelet analysis, a compact presentation of field experiments data was obtained in the form of amplitude-frequency characteristics, which provides the possibility of qualitative and quantitative analysis of the discontinuous yield. Type B bands are characterized by the presence of one pronounced frequency on the scalogram and appear at characteristic jumps frequency of 2.0 – 8.0 Hz, type A bands, due to their lower frequency (3.5 Hz), appear as noise (low-frequency oscillations) with smaller amplitudes. The presented results of processing experimental data using wavelet analysis indicate the effectiveness of this mathematical apparatus for the qualitative and quantitative analysis of the Portevin–Le Chatelier effect.

ACKNOWLEDGES

Mechanical tests were performed at the Center for Experimental Mechanics using the Unique Scientific Installation "Complex of testing and diagnostic equipment for studying the properties of structural and functional materials under complex thermomechanical effects".
The study was carried out with a financial support from the Ministry of Education and Science of the Russian Federation as part of the implementation of the national project "Science and Universities" (the state task fulfillment in the laboratory of multilevel structural and functional materials modeling, project no. FSNM-2021-0012).

REFERENCES

[1] Ait-Amokhtar, H. and Fressengeas, C. (2010). Crossover from continuous to discontinuous propagation in the Portevin – Le Chatelier effect, Acta Mater., 58, pp.1342-1349. DOI: 10.1016/j.actamat.2009.10.038.
[2] Benallal, A., Berstad, T., Børvik, T., Hopperstad, O.S. and Nogueira de Codes, R. (2008a). Effects of strain rate on the characteristics of PLC deformation bands for AA5083-H116 aluminium alloy, Philos. Mag., 88(28-29), pp.3311-3338. DOI: 10.1080/14786430802468223.
[3] Casarotto, L., Dierke, H., Tutsch, R. and Neuhäuser, H. (2009). On nucleation and propagation of PLC bands in an Al–3Mg alloy, Mater. Sci. Eng. A., 527, pp.132-140. DOI: 10.1016/j.msea.2009.07.043.
[4] Coër, J., Manach, P.Y., Laurent, H., Oliveira, M.C. and Menezes, L.F. (2013). Piobert–Lüders plateau and Portevin–Le Chatelier effect in an Al–Mg alloy in simple shear, Mech. Res. Commun., 48, pp.1-7. DOI: 10.1016/j.mechrescom.2012.11.008.
[5] Halim, H., Wilkinson, D.S. and Niewczas, M. (2007). The Portevin – Le Chatelier (PLC) effect and shear band formation in an AA5754 alloy, Acta Mater., 55, pp.4151-4160. DOI: 10.1016/j.actamat.2007.03.007.
[6] Molland, A.F. and Turnock, S.R. (2022). Marine Rudders, Hydrofoils and Control Surfaces: Principles, Data, Design and Applications (Second Edition), 546 pp. DOI: doi:10.1016/C2020-0-01238-7.
[7] Tretyakova, T.V. (2014). Features of the use of VIC-3D software, which implements the digital image correlation method, as applied to the study of inelastic deformation fields, Computational continuum mechanics, 7(2), pp. 162-171. DOI: 10.7242/1999-6691/2014.7.2.17.
[8] Benallal, A., Berstad, T., Børvik, T., Hopperstad, O.S. and Nogueira de Codes, R. (2008b). On the measurement and evaluation of the width of Portevin–Le Chatelier deformation bands with application to AA5083-H116 aluminium alloy, In: IUTAM Symposium on Theoretical Modelling and Computational Aspects of Inelastic Media, B.D. Reddy (ed.), Springer Science+Business Media B.V., pp.329-338. DOI: 10.1007/978-1-4020-9090-5_30.
[9] Sun, L., Zhang, Q. and Cao, P. (2009). Infuence of solute cloud and precipitates on spatiotemporal characteristics of Portevin – Le Chatelier effect in A2024 aluminum alloys, Chinese Physics B, 18(8), pp.3500-3507. DOI: 10.1088/1674-1056/18/8/061.
[10] Zhang, Q., Jiang, Z., Jiang, H., Chen, Z. and Wu, X. (2005). On the propagation and pulsation of Portevin – Le Chatelier deformation bands: An experimental study with digital speckle pattern metrology, Int. J. Plast., 21, pp.2150–2173. DOI:10.1016/j.ijplas.2005.03.017.
[11] Ranc, N. and Wagner, D. (2005). Some aspects of Portevin – Le Châtelier plastic instabilities investigated by infrared pyrometry, Mater. Sci. Eng. A., 394, pp.87-95. DOI: 10.1016/j.msea.2004.11.042.

[12] Scavino, G., Di, Salvo, C., Matteis, P., Sesana, R. and Firrao D. (2013). Portevin – Le Chatelier effects in a high-Mn austenitic steel, Metal. Mater. Trans. A, 44(2), pp. 787-792. DOI:10.1007/s11661-012-1445-5.
[13] Li, X., Xu, Z., Guo, P., Peng, L. and Lai, X. (2022). Electroplasticity mechanism study based on dislocation behavior of Al6061 in tensile process, J. Alloys Compd, 910, 164890 (13 p.). DOI: 10.1016/j.jallcom.2022.164890.
[14] Sarkar, A., Barat, P. and Mukherjee, P. (2013). Investigation of Portevin–Le Chatelier effect in Al-2.5 pct Mg alloy with different microstructure, Metal. Mater. Trans. A, 44A, pp.2604-2012. DOI: 10.1007/s11661-013-1630-1.
[15] Vani Shankar, Valsan, M., Bhanu Sankara Rao K. and Mannan, S.L. (2004). Effects of temperature and strain rate on tensile properties and activation energy for dynamic strain aging in alloy 625, Metal. Mater. Trans. A, 35A, pp.3129-3139. DOI: 10.1007/s11661-004-0057-0.
[16] Wang, W., Wu, D., Chen, R. and Lou, C. (2015). Influence of temperature and strain rate on serration type transition in NZ31 Mg alloy, T. Nonferr. Metal. Soc., 25, pp.3611-3617. DOI: 10.1016/S1003-6326(15)64002-X.
[17] Yavorsky, B. M. and Pinsky, A. A. (1974). Fundamentals of Physics. 2 [Osnovi fiziki. Tom 2], M.: Nauka, 180 p.
[18] Yilmaz A. (2011) The Portevin – Le Chatelier effect: a review of experimental findings, Sci. Technol. Adv. Mater. 12, pp 063001 – 063017. DOI:10.1088/1468-6996/12/6/063001.
[19] Brechtl, J., Chen, B., Xie, X., Ren, Y., Venable, J.D., Liaw, P.K. and Zinkle, S.J. (2019). Entropy modeling on serrated flows in carburized steels,Mater. Sci. Eng. A., 753, pp.135-145. DOI: 10.1016/j.msea.2019.02.096.
[20] Darowicki, K., Orlikowski, J. and Zieliński, A. (2008). Frequency bands selection of the Portevin – Le Chatelier effect, Comput. Mater. Sci., 43, pp.366-373. DOI:10.1016/j.commatsci.2007.12.001.
[21] Chmelik, F., Pink, E., Król, J., Balik, J., Pešička, J. and Lukáč, P. (1998). Mechanisms of serrated flow in aluminium alloys with precipitates investigated by acoustic emission, Acta mater, 46(12), pp. 4435-4442. DOI: 10.1016/S1359-6454(98)00070-6.
[22] Härtel, M., Illgen, C., Frint, P. and Wagner, M.F.-X. (2018). On the PLC effect in a particle reinforced AA2017 alloy, Metals, 8(2), pp.1-13. DOI: 10.3390/ met8020088.
[23] Lebyodkin, M.A., Kobelev, N.P., Bougherira, Y., Entemeyer, D., Fressengeas, C., Gornakov, V.S., Lebedkina, T.A. and Shashkov, I.V. (2012). On the similarity of plastic flow processes during smooth and jerky flow: Statistical analysis, Acta Mater., 60, pp.3729-3740. DOI: 10.1016/j.actamat.2012.03.026.
[24] Lukáč, P., Balik, J. and Chmelik, F. (1997). Physical aspects of plastic instabilities, Mater. Sci. Eng. A.,234-236, pp.45-51. DOI: 10.1016/S0921-5093(97)00178-0.
[25] Lindgren, L.-E., Domkin, K. and Hansson, S. (2008). Dislocations, vacancies and solute diffusion in physical based plasticity model for AISI 316L, Mech. Mater., 40, pp. 907–919. DOI: 10.1016/j.mechmat.2008.05.005.
[26] Shibkov, A.A., Zolotov, A.E., Zheltov, M.A., Denisov, A.A. and Gasanov, M.F. (2014). Macrolocalization of plastic deformation during intermittent creep of aluminum-magnesium alloy AMg6 [Makrolokalizatsiya plasticheskoi deformatsii pri prerivistoi polzuchesti alyuminii-magnievogo splava AMg6], J. Tech. Phys., 84(4), pp.40-46.
[27] Tretyakova, T.V., Tretyakov, M.P. and Chechulina, E.A. (2021). Experimental study of the Portevin-Le Chatelier effect under complex loading of Al-Mg alloy: procedure issues, Frat. ed Integrità Strutt., 58, pp. 434-441. DOI: 10.3221/IGF-ESIS.58.31.
[28] Brindley, B.J. and Worthington, P.J. (1970). Yield-point phenomena in substitutional alloys, Metallurgical Reviews, 15(1), pp.101-114. DOI: 10.1179/mtlr.1970.15.1.101.
[29] Chihab, K., Estrin, Y., Kubin, L.P. and Vergnol, J. (1987). The kinetics of the Portevin – Le Chatelier bands in an Al–5at%Mg alloy, Scripta Metallurgica, 21(2), pp.203-208. DOI: 10.1016/0036-9748(87)90435-2.
[30] Cuddy, L.J. and Leslie W.C. (1972). Some aspects of serrated yielding in substitutional solid solutions of iron, Acta Metallurgica, 20(10), pp.1157-1167. DOI: 10.1016/0001-6160(72)90164-2.
[31] Jiang, H., Zhang, Q., Chen, X., Chen, Z., Jiang, Z., Wu, X. and Fan J. (2007). Three types of Portevin–Le Chatelier effects: Experiment and modelling, Acta Mater., 55(7), pp.2219-2228. DOI: 10.1016/j.actamat.2006.10.029.
[32] Russell, B. (1963). Repeated yielding in tin bronze alloys, Phil. Mag. J. Theor. Exp. Appl. Phys., 88(8), pp.615-630. DOI: 10.1080/14786436308211160.
[33] Schwink, Ch. and Nortmann, A. (1997). The present experimental knowledge of dynamic strain ageing in binary f.c.c. solid solutions, Mater. Sci. Eng. A., 234 – 236, pp.1-7. DOI: 10.1016/S0921-5093(97)00139-1.
[34] Tamimi, S., Andrade-Campos, A. and Pinho-da-Cruz, J. (2015). Modelling the Portevin – Le Chatelier effects in aluminium alloys: a review, J. Mech. Behav. Mater., 24(3-4), pp.67-78. DOI: 10.1515/jmbm-2015-0008.
[35] Bharathi, M.S., Lebyodkin, M., Ananthakrishna, G., Fressengeas, C. and Kubin, L.P. (2001). Multifractal burst in the spatio-temporal dynamics of jerky flow, Phys. Rev. Lett., 87, pp.165508. DOI: 10.1103/PhysRevLett.87.165508.
[36] Bharathi, M.S., Lebyodkin M., Ananthakrishna G., Fressengeas C., Kubin L.P. (2002). The hidden order behind jerky flow, Acta Mater.,50, pp.2813-2824. DOI: 10.1016/S1359-6454(02)00099-X.

[37] Cetlin, P.R. and Güleç, A.Ş., Reed-Hill R.E. (1973). Serrated flow in aluminum 6061 alloy, Metal. Trans, 4, pp.513-517 (1973). DOI: 10.1007/BF02648704.
[38] Chihab, K., Ait-Amokhtar, H. and Bouabdellah, K. (2002). Serrated yielding due to Portevin – Le Chatelier effect in commercial Al-Mg alloys, Ann. Chim. Sci. Mat., 27, pp.69-75. DOI:10.1016/S0151-9107(02)85008-5.
[39] Ranc, N. and Wagner, D. (2008). Experimental study by pyrometry of Portevin – Le Châtelier plastic instabilities—Type A to type B transition, Mater. Sci. Eng. A., 474, pp. 188-196. DOI: 10.1016/j.msea.2007.04.012.
[40] Chatterjee, A., Sharma, G., Tewari, R. and Chakravartty, J.K (2015). Investigation of the Dynamic strain aging and mechanical properties in alloy-625 with different microstructures, Metal. Mater. Trans. A, 46A, pp.1097-1107. DOI: 10.1007/s11661-014-2717-z.
[41] Chihab, K. and Fressengeas, C. (2003). Time distribution of stress drops, critical strain and crossover in the dynamics of jerky flow,Mater. Sci. Eng. A., 356, pp.102-107. DOI: 10.1016/S0921-5093(03)00141-2.
[42] Mehenni, M., Ait-Amokhtar, H. and Fressengeas, C. (2019). Spatiotemporal correlations in the Portevin-Le Chatelier band dynamics during the type B – type C transition, Mater. Sci. Eng. A., 756, pp.313-318. DOI: 10.1016/j.msea.2019.04.036.
[43] Rodriguez, P. (1984). Serrated plastic flow, Bull. Mater. Sci., 6(4), pp.653-663. DOI:10.1007/BF02743993.
[44] Trusov, P.V., Wildemann, V.E., Chechulina, E.A., Tretyakova, T.V. and Tretyakov, M.P. (2022). Influence of a complex loading on a behavior of an aluminum alloy within the framework of the Portevin – Le Chatelier effect, Procedia Structural Integrity, 40, pp.433–439. DOI: 10.1016/j.prostr.2022.04.058.
[45] Dyakonov, V.P. (2002). Wavelets. From theory to practice [Veivleti. Ot teorii k praktike], M.: SOLON-R, 448 p.
[46] Novikov, L.V. (1999). Fundamentals of wavelet signal analysis: Textbook [Osnovi veivlet-analiza signalov: Uchebnoe posobie], St. Petersburg, IAnI RAS, 152 p.
[47] Astafeva, N.M. (1996). Wavelet analysis: basic theory and some application. Phys. Usp., 166 (11), pp. 1145-1170.
[48] Goupillaud, P., Grossman, A. and Morlet, J. (1984). Cycle-Octave and Related Transforms in Seismic Signal Analysis, Geoexploration, 23(1), pp. 85-102. DOI: 10.1016/0016-7142(84)90025-5.
[49] Dremin, I.L. and etc. (2001). Wavelet and their uses [Veivleti i ikh ispolzovanie], Phys. Usp., 171 (5), pp. 465-501. DOI: 10.1070/PU2001v044n05ABEH000918.